Basin Compartmentalization in the Sierra Pampeanas of Northwestern Argentina: Case-study of the El Cajón Basin.

Jonathan R. Pratt, Lindsay Schoenbohm, Estelle Mortimer & Axel Schmitt

Senior Thesis

Completed 12/8/08

As partial requirement for a B.S. in Geological Sciences

Research Advisor: Lindsay Schoenbohm

Basin Compartmentalization in the Sierra Pampeanas of Northwestern Argentina: Case-study of the El Cajón Basin.

Jonathan R. Pratt, Lindsay A. Schoenbohm, Estelle Mortimer and Axel Schmitt

Abstract

In order to characterize the propagation of an orogenic wedge into the foreland in a thick-skinned setting, the El Cajón Basin in Northwestern Argentina was chosen as the locale for a case-study. The El Cajón Basin serves this purpose well as it has previously been incorporated into the morphologic Puna Plateau of the Central Andes and has since been exhumed. The exhumation of the basin allows the study of deformation within the basin's three allostratigraphic formations, the Peñas Azules, the Playa del Zorro and the Totoral formations. Two cross-sections have been generated in this study from geologic mapping of the basin and are coupled with previously interpreted seismic data from the Campo del Arenal Basin, just south of the El Cajón Basin. These data and new U-Pb geochronology of tuff beds within the basin stratigraphy allow a more comprehensive understanding of the temporal and spatial evolution of the El Cajón Basin in a regional context. Of particular interest is the timing of uplift for the Sierra de Chango Real, the western bounding range of the El Cajón, the Sierra de Quilmes, a basement-cored anticline that separates the El Cajón Basin from the Santa María Basin to the east, and the Sierra Aconquija, which separates these intermontane basins from the foreland to the east. The new U-Pb ages indicate an in-sequence pattern of deformation across the foreland, with the Sierra de Chango Real uplift at 13.6 Ma and the Sierra de Quilmes at ~8-12 Ma as determined from this study, and the Sierra Aconquija at ~6 Ma [Sobel & Strecker, 2003]. The Sierra de Quilmes is also shown to have propagated from N to S, consistent with predictions based on the oblique-angle subduction of the Juan de Fernandez ridge beneath the South American plate. Geologic evidence shows that deformation is largely controlled by pre-existing basement fabrics and faults, with high-angle reverse faults as the dominant mode of shortening. Together these data provide a model for an east to west in-sequence propagation of the orogenic wedge with a north to south influence that is largely controlled by pre-existing basement structures. Each progressive uplift compartmentalized a piece of the foreland into a basin that was then filled and incorporated into the plateau, a model of orogenic wedge propagation vastly different from those seen in thin-skinned settings.

1.1 Introduction

Models of deformation in "thin-skinned" settings largely define understanding of the mechanisms by which the continental crust incorporates the foreland into an active orogen during compression. In the Coulomb-wedge model, thrusts and folds propagate through the sedimentary rocks overlying the basement utilizing weaknesses in bedding planes at low angles [Davis et al., 1983, Dahlen et al., 1984] and advance as a front that "pushes" the flexural foreland as the thrust wedge itself advances [Decelles & Giles, 1996]. Basins are incorporated into the wedge top if wedge propagation out-competes flexural subsidence.

[Decelles & Giles, 1996] In these settings the foreland is usually deformed in-sequence, meaning that active faults are always at the tip of the wedge and become inactive as the wedge migrates, initiating new faults in the direction of propagation [Decelles & Giles, 1996]. Basement is uplifted in this setting only if it is incorporated into successive thrust sheets, each bringing more material towards the surface, including older thrust wedges [Schmitt & Steidtmann, 1990] and is not of major significance to the style of deformation.

This model does not apply well to thick-skinned settings where faults do not rely on bedding planes to reach the surface. In these settings faults are typically high angle, and cause basement uplift as faults exploit pre-existing weaknesses in the crystalline basement. Basement-cored uplift through thick-skinned faulting and folding creates localized loading and flexure, fragmenting the foreland and incorporating it into the orogen, with deformation often occurring out-of-sequence [Mortimer et al., 2007]. In thick-skinned tectonic settings, such as that found in the Puna Plateau, plateaus may form from a succession of basement uplifts moving into the foreland. Basins between the uplifts can become closed and fill with sediment, becoming part of the internally drained, low-relief, high elevation plateau. This mechanism by which fragmenting of the foreland occurs is vastly different from the thin-skinned model, in which migration of the wedge is continuous and crustal thickening occurs through successive stacking of thrust sheets. To better resolve the mechanisms by which these plateaus are formed, to understand the structural, spatial and temporal variance in their formation, and to elucidate the differences between thin- and think-skinned propagation, more data are needed from deforming forelands in a thick-skinned setting.

This study focuses on the El Cajón basin of northwest Argentina. The El Cajón lies along the eastern margin of the Puna Plateau and is bounded by basement uplifts on both the

western and eastern side. The basin is partially filled by a clastic sequence, suggesting it was once hydrologically isolated, and therefore morphologically linked to the modern, internally drained Puna plateau. Since then, however, it has been incised and reincorporated into the foreland [Sobel & Strecker, 2003]. The basin contains a Miocene-Pliocene sedimentary sequence that records the compartmentalization of the basin both temporally through intercalated tuff beds and structurally through the sedimentary sequence and deformation. These attributes make the El Cajón basin an ideal site for a case study focusing on how the foreland is incorporated into an active orogen in a thick-skinned setting.

2. Geologic Background

2.1 Geography

The El Cajón basin lies between 66°35'0"W and 66°15'0"W and 26°30'0"S and 26°55'0"S, situated along the eastern margin of the Puna plateau in the Sierras Pampeanas structural province (Fig. 1). The plateau floor is ~ 3700 m in mean elevation [Isacks, 1988] and the floor of the El Cajón basin is ~2500 m. The eastern boundary of the Puna plateau is the Sierra de Chango Real. East of this range lies the Sierra de Quilmes and further east the Sierra Aconquija. The foreland stretches east from the Sierra Aconquija towards the Atlantic Ocean, with the Sierra Aconquija and the Cumbres Calchaquies to the north being the easternmost ranges along an E-W transect. Between the Sierra de Chango Real and the Sierra Aconquija/Cumbres Calchaquies are the marginal foreland basins that represent the transitional phase between the undeformed foreland and the plateau proper. These basins are the Hualfín Basin, the El Cajón -Campo del Arenal Basin and the Santa María Basin. Uplifted basement rocks of the Sierra de Quilmes and the Sierra de Hualfín separate these

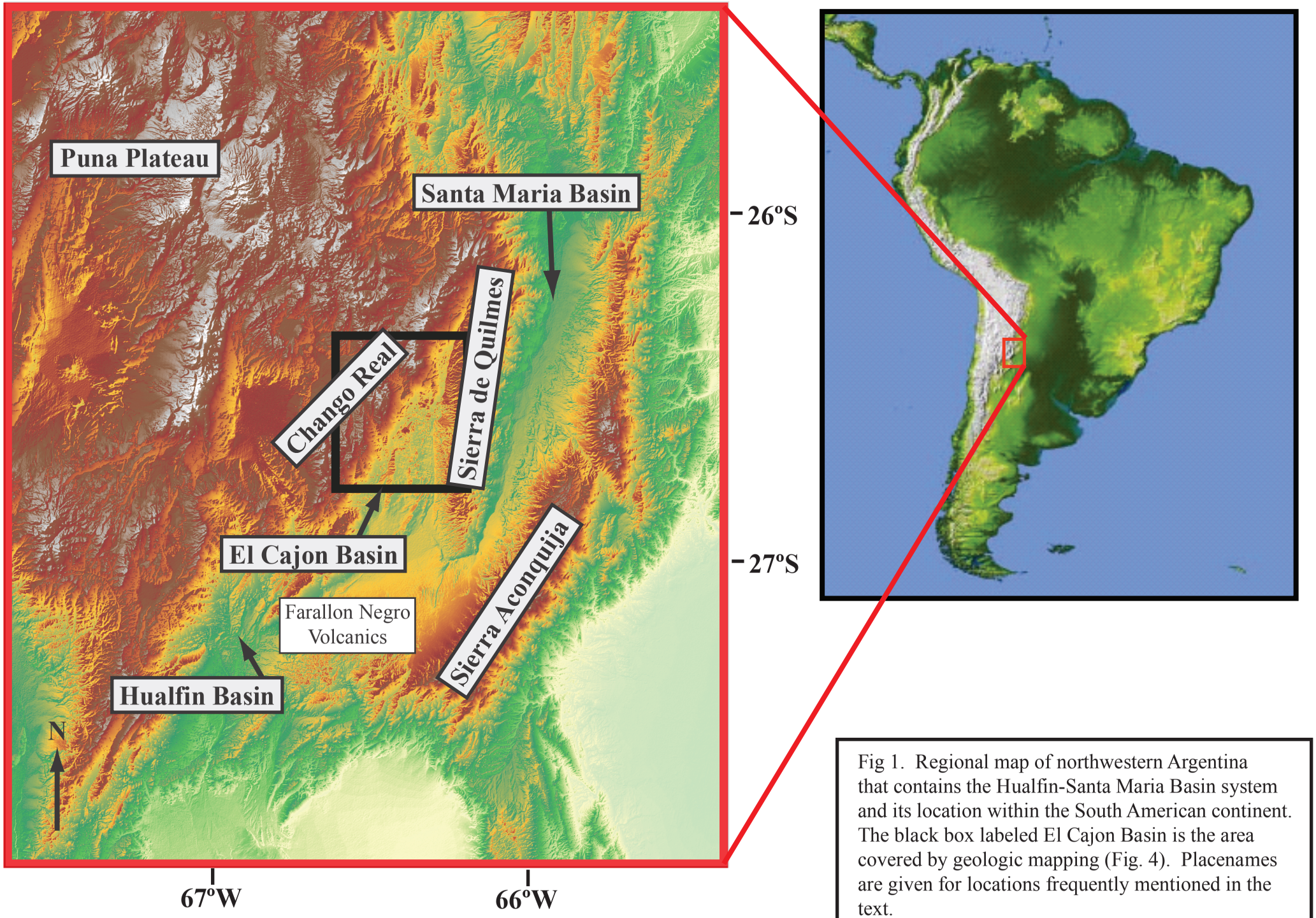

Fig 1. Regional map of northwestern Argentina that contains the Hualfin-Santa Maria Basin system and its location within the South American continent. The black box labeled El Cajon Basin is the area covered by geologic mapping (Fig. 4). Placenames are given for locations frequently mentioned in the text.

basins from one another. All of the basins drain to the Atlantic Ocean, though there is a divide, with the El Cajón -Campo del Arenal and Santa María basins draining north through the Santa María and the Hualfín draining south. The basins are arid due to precipitation being blocked from the east by the Aconquija and Cumbres Calchaquies topographic barriers. The El Cajón basin, which is the focus of this study, is a subbasin of the El Cajón - Campo del Arenal basin. It is closed to the north by the intersection of the Sierra de Chango Real and the Sierra de Quilmes and extends south to the southernmost tip of the Sierra de Quilmes and west to the Sierra de Chango Real. South of this extent is where the Campo del Arenal subbasin begins. The El Cajón portion of the basin is chosen for this study largely due to greater stratigraphic exposure. The El Cajón basin is in geologic "limbo," neither truly part of the plateau or the foreland, but instead it is in-between, making it an optimal location for studying how plateaus grow.

2.2 Tectonics and Structure

2.2.1 Regional Tectonic Setting

The El Cajón Basin lies in the foreland of the Pampean flat-slab segment (27°00'-33°30'S) of the subduction zone between the Nazca plate and the South American plate. More specifically it lies in the northern Sierras Pampeanas structural province, the southern portion of the Puna Plateau and the portion of the Andes closest to the foreland along and E-W transect. The Pampean flat-slab segment of the subduction zone is characterized by a gap in arc volcanism in the Andes along the trench axis and the basement-block faulted foreland of which the El Cajón is a part. The shallow subduction extends the lateral distance at which the subducting plate reaches a depth where the dehydration of the oceanic plate can occur

and initiate arc volcanism [Ramos et al., 2002]. The inferred cause of the plate shallowing is the subduction of the more buoyant Juan de Fernandez volcanic arc, which occurred around 11 Ma at this latitude with the collision propagating from N-S [Ramos et al., 2002].

Ramos et al [2002] cite the migration of arc volcanism in the foreland, itself caused by flat-slab subduction, as the cause for the thick-skinned tectonic regime that occurs in the area. Thermal weakening of the crust by arc volcanism elevates the depth of the brittle-ductile detachment surface. With the detachment surface elevated, crustal failure through compression takes place in a thick-skinned regime, forming the high-angle, basement-involved reverse faults that form the basement blocks that are characteristic of the Sierra Pampeanas structural province [Ramos et al., 2002]. The El Cajón -Campo del Arenal basin is bounded by such high-angle, basement-involved reverse faults.

The Sierra Pampeanas province has undergone several compressional and extensional events in its history that all play a role in developing the style of deformation in the region. It begins with the compressional events that formed the western margin of Gondwana in the late Proterozoic to early Paleozoic [Ramos et al., 2002]. These events created a pervasive foliation and schistosity [Toselli et al., 1985; Von Gosen, 1998] in the crystalline basement that largely controlled the nature of later deformation within the region [Ramos et al., 2002]. Three extensional events followed in the late Paleozoic, late Triassic-early Jurassic and the early Cretaceous, all reactivating pre-existing structures [Ramos et al., 2002]. Most important of these for the El Cajón Basin is the early Cretaceous Salta rifting event. It is generally agreed upon that the Cretaceous Salta rift normal faults and the basement fabric developed in the Gondwana collisional event controlled the location and geometry of the faulting that later occurred in the Cenozoic during Sierras Pampeanas deformation [Ramos et

al., 2002; Mortimer et al., 2007; Strecker et al., 1989] and hence the compartmentalization of the Hualfín-Santa María basin system.

2.2.2 Structural geology of the El Cajón Basin

The El Cajón Basin is within the northernmost extent of the Sierras Pampeanas as part of the Puna terrane where it overrides the Pampia terrane [Ramos et al., 2002]. The volcanism responsible for crustal weakening in this portion of the Sierras Pampeanas is expressed by the Farallon Negro volcanic complex, located south of the Campo del Arenal Basin [Ramos et al., 2002]. This area differs from that further south where west-vergent faulting is dominant. In the study region, the faulting across the Sierras Pampeanas is approximately equally divided between east and west vergence [Ramos et al., 2002] (Fig. 2). The Chango Real east-vergent reverse fault bounds the El Cajón and the Hualfín-Santa María system as a whole to the east. The Sierra Aconquija reverse fault is west-vergent and bounds the basin system to the east. In between these faults lies the Sierra de Quilmes south-plunging basement-cored anticline.

A master fault that controls the uplift of the Sierra de Quilmes does not outcrop, however the seismic data of *Mortimer et al.* [2007] south of the Sierra de Quilmes in the Campo del Arenal Basin show both a west-vergent and an east-vergent fault coring the anticline (Fig. 3). This places the Sierra de Quilmes in the transition zone between two fault trends of opposite vergence (the Chango Real and Aconquija). Although to date it can only be inferred that the Sierra de Quilmes in outcrop exhibits the same structural style as in the seismic data to the south, the seismic data is consistent with the basement folding mechanisms described by *Garcia & Davis* [2004]. They describe a model in which basement

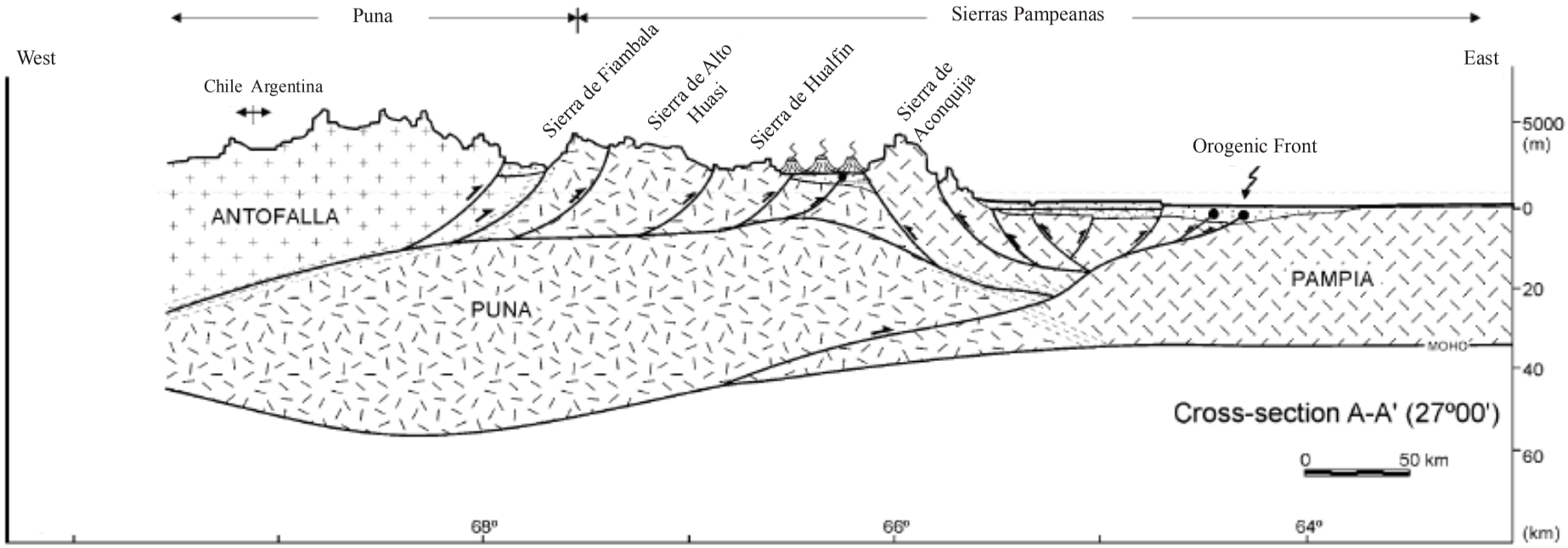

Fig. 2: Cross-section taken directly from *Ramos et al. 2002*. Cross-section line passes through the Farallon Negro volcanic complex, just south of the El Cajon Basin, showing regional structure.

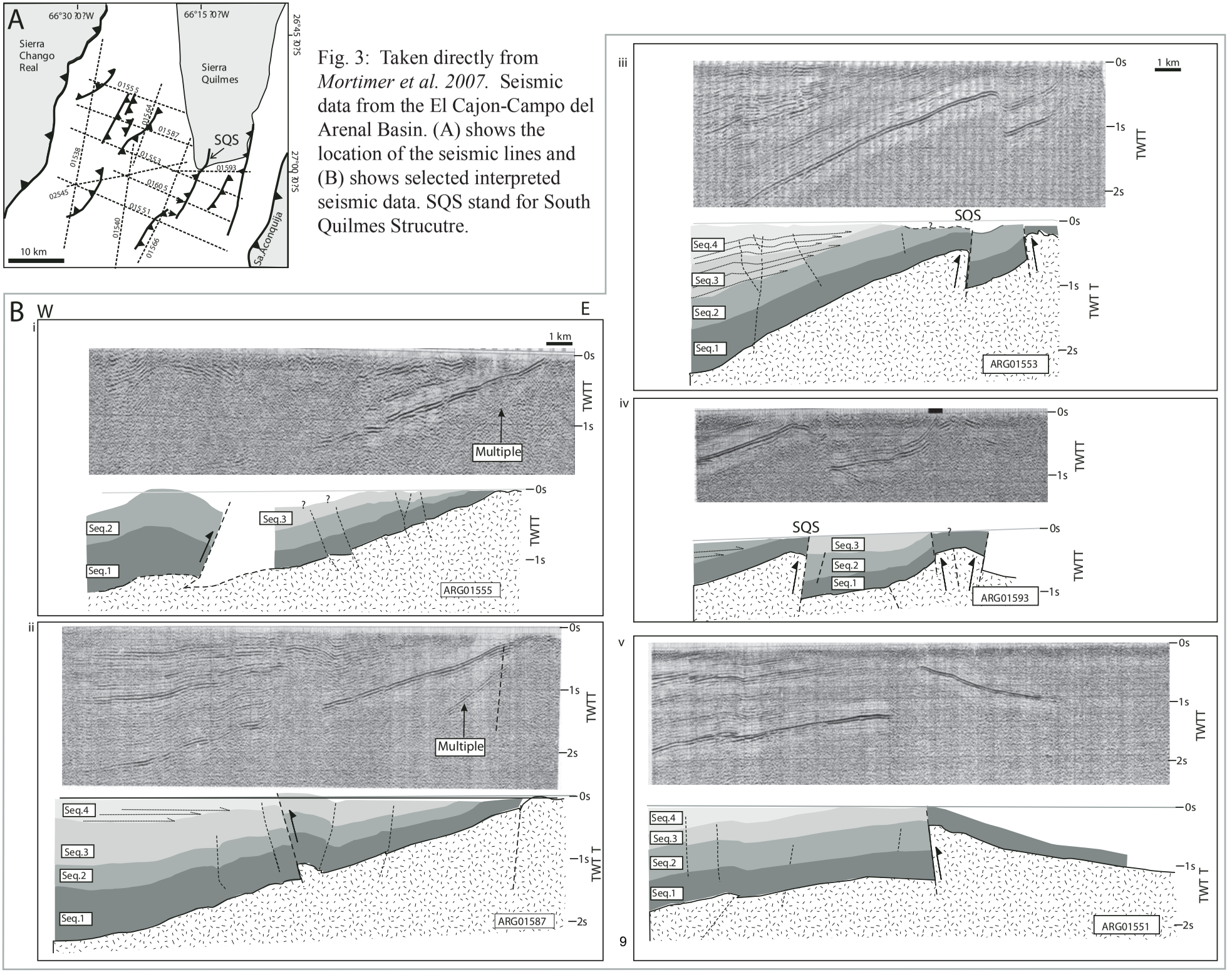

Fig. 3: Taken directly from *Mortimer et al. 2007.* Seismic data from the El Cajon-Campo del Arenal Basin. (A) shows the location of the seismic lines and (B) shows selected interpreted seismic data. SQS stand for South Quilmes Strucutre.

is folded through the reactivation of joints as faults and flexural shear in the uppermost part of the basement that is consistent with trishear mechanics. While *Garcia & Davis* [2004] studied the intrusive granitic rock of the Sierra de Hualfín (located adjacent to the Hualfín basin), the same model can be applied to the metamorphic basement rocks of the Sierra de Quilmes, which, instead of penetrative jointing, contain the pervasive foliations and weaknesses associated with the region. The shift in fault vergence across the region may reflect changes in the basement fabric, with greater variability in the area of the Sierra de Quilmes.

A second bimodal distribution of structure occurs in the Hualfín-Santa María basin system. The Chango Real and Sierra Aconquija basement reverse faults both strike approximately N25E whereas the Sierra de Quilmes and Cumbres Calchaquies strike almost exactly N-S. The differing trend of the Sierra Aconquija is thought to be the result of the a 100-km-wide dextral transpressive zone known as the Tucuman transfer zone that accommodated the differing rates of crustal shortening between the Puna-Subandean system and the Principal Cordillera-Precordillera-Sierras Pampeanas system [Ramos et al., 2002; Ramos, 1977; Urreiztieta et al., 1996]. The Hualfín-Santa María basin system is on the boundary of two different structural transitions, making it a structurally dynamic place to study basin evolution.

2.3 Sedimentology and Stratigraphy

The sedimentary sequence in the El Cajón basin is divided into three alloformations with disconformable boundaries that exhibit spatial variance in the intensity of the unconformity; the Peñas Azules Formation, the Playa del Zorro Formation and the Tortoral

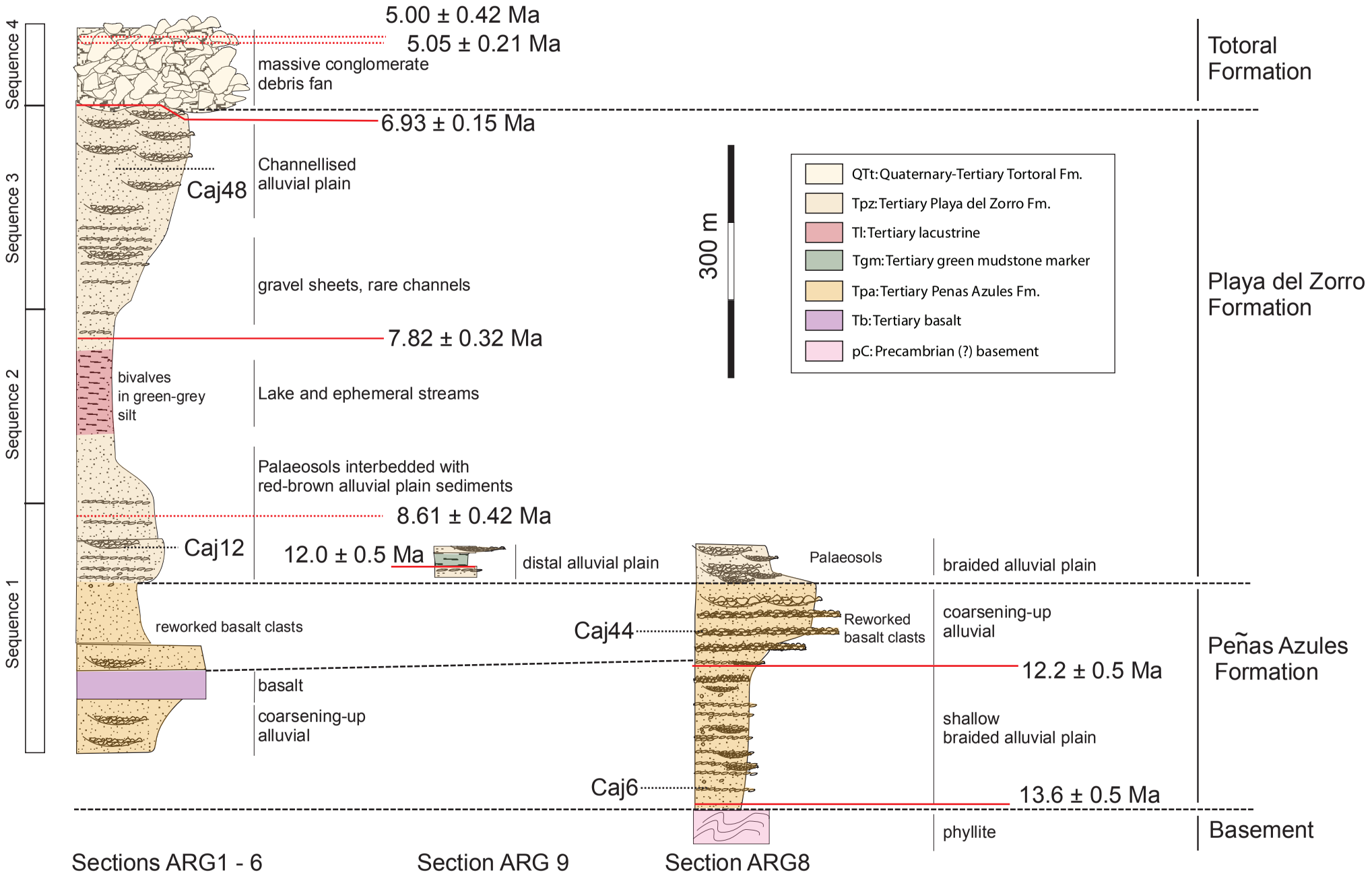

Fig 4. Allostratigraphic column produced by *Mortimer et al* [2007] that has been updated by Estelle Mortimer since publication to reflect new zircon age dates as determined by this author.

Formation (or Playa del Tortoral) (Fig. 4) [Bossi et al., 1999]. *Bossi et al.* [1999] cite long-term variations in tectonic behavior for the formation boundaries and recognize each formation as a distinct drainage stage.

The shallowly dipping peneplain on which the El Cajón sedimentary package rests is composed primarily of crystalline phyllites [Bossi et al., 1997] containing schistosity that is nearly vertical with an attitude of N66°E, 70°E [Bossi et al., 2000]. The surface records a paleowind direction of N212°E determined from smooth surfaces facing that direction and pitted surfaces facing away [Bossi et al., 1997].

Overlying the peneplain is the Peñas Azules Fm. The formation is a coarsening-upwards alluvial sequence composed of fine sandstones and coarse siltstones that pass laterally into lenticular conglomerates [Mortimer et al., 2007]. Most of the material is derived from intermediate to low-grade metamorphic Precambrian to lower Paleozoic basement rocks [Bossi et al., 2000] while larger sand grains and pebbles are volcanic in origin [Mortimer et al., 2007, Bossi et al., 2000]. The unit contains a 10-30 m thick [Mortimer et al, 2007] basalt layer that is cited to be both near the base [Bossi et al, 2000] and near the top [Mortimer et al., 2007] of the unit. The different placements of the basalt layer within the unit are likely the result of different locations of observation, which would indicate varying thickness of the sedimentary rocks underlying the basalt. If this is true, then it is likely that the formation is time-transgressive, with the greater sedimentary thickness at the time the basalt was laid down closer to the depocenter. *Bossi et al.* [200] measured a mean paleocurrent direction of E-ESE with low variance that extends through the present-day location of the Sierra de Quilmes which, along with a lack of variance in pebble size from N-

S, serves as evidence of a continuous alluvial plain between the present-day El Cajón -Camp del Arenal and Santa María basins [Bossi et al., 2000].

The Peñas Azules Fm. and the overlying Playa del Zorro Fm. are separated by an erosive unconformity, which varies in angularity, indicating syn-depositional deformation [Mortimer et al., 2007, Bossi et al., 1997]. The Playa del Zorro is a coarsening-upwards sequence of sandstones that increase progressively upsection to more conglomeritic deposits [Bossi et al., 1997]. A lacustrine unit within the formation is composed of mudstones and muddy sandstones containing 1-3cm gypsum beds, bivalves and rare coarser cross-bedded sandstones [Mortimer et al., 2007]. *Mortimer et al*. [2007] interpret the gypsum beds and cross-bedded sandstones to indicate periodic drying of the lake. Pebble composition is primarily volcanic in the north from sources to the N and W, with a greater concentration of plutonic and metamorphic pebbles further south in the basin [Bossi et al., 2000]. The drainage is again of low variance at the regional scale but with an increase in channel sinuosity. This indicates a lower gradient across the basin with paleocurrent direction deflected to the SE [Bossi et al., 2000].

The upper boundary of the Playa del Zorro Fm. is a more regional angular unconformity than its lower boundary, above which lies the Tortoral (or Playa del Tortoral) Fm. The lithology is dominated by boulder-cobble sheet conglomerates and boulder-rich lenticular conglomerates interbedded with medium-grained, massive and cross-bedded sandstones [Mortimer et al., 2007]. Drainage direction during the deposition of the Tortoral Fm. diverted southwards, either around the Sierra de Quilmes and into the Santa María Basin or continuing south in the Campo del Arenal Basin, indicating significant elevation along the

present-day Sierra de Quilmes at that time [Bossi et al., 2000]. *Bossi et al.* [2000] view this formation as reflecting the climax of compressive tectonics and mountain uplift in the area.

This stratigraphic sequence is recognized to apply to the Hualfín-Santa María basin system as a whole and is correlated to the older lithoformation names by *Bossi et al.* [1997]. Differences do exist between the El Cajón basin stratigraphy and that of the Santa María basin. While it is not the aim of this study to evaluate the sedimentological differences between the basins, certain discrepancies serve to point out the shift from a continuous basin to a fragmented basin. The first point lies within the Corral Quemado lithoformation, which is equivalent to the upper portion of the Playa del Zorro alloformation [Bossi et al., 1997]. *Strecker et al.* [1989] state that in the Santa María Basin, transport direction is to the west in the Corral Quemado and the composition is derived from basement to the east (Sierra Aconquija/Cumbres Calchaquies). This is in contrast to the transportation direction found in the El Cajón, which was to the southeast [Bossi et al., 2000] in the equivalent Playa del Zorro Fm. The equivalent units in either basin are being derived from different sources and being transported in different directions, suggesting basin compartmentalization by this time. Further supporting this, the Yasyamayo Fm., which is equivalent to the Tortoral [Bossi et al., 1997] has different characteristics in either basin. In the El Cajón, it is a more massive conglomerate, whereas in the Santa María the unit consists of a lower fine-medium grained sandstone with conglomeratic lenses and an upper fine-medium sandstone with gypsum and pelite horizons and in some portions of the basin more closely resembles the blocky conglomerates of the El Cajón [Strecker et al., 1989]. The differences in stratigraphy between the two basins clearly contain key evidence for understanding the fragmentation of

the basin. However, to understand the process temporally, better age constraints are required for the stratigraphy of the El Cajón Basin.

3. New Geologic Mapping and Cross-sections of the El Cajón

New geologic mapping [Schoenbohm, pers. comm.] of the El Cajón basin has provided the opportunity for a more comprehensive analysis of the intra-basin structure (Fig. 5). From this mapping, two rigorous cross-sections were created using the kink-band (dip domain) method [Suppe, 1985]. All dips were converted to apparent dips. Due to the changing thickness of each unit across the basin, the cross-sections could not be conventionally balanced using the equal line length method. Sound geologic interpretations of subsurface structure were synthesized from surface exposure, seismic data from the Campo del Arenal Basin and models of trishear and fault-propagation folding. Despite the lack of mathematical balancing, the cross-sections are valuable tools that provide insight into the style and chronology of deformation.

Two cross-section lines were chosen based on the amount of exposure and data available from the geologic mapping. One line (A-A') was taken from the northern half of the basin and the other (B-B') was taken from the middle. These two cross-sections in combination with the interpreted seismic data from *Mortimer et al.* [2007] provide a north to south sequence of subsurface interpretation that provide insight into the structural and sedimentary response within the El Cajón Basin to the uplift of the Sierra de Quilmes basement-cored anticline and therefore also shed light onto the process by which the El Cajón was cut off from the foreland.

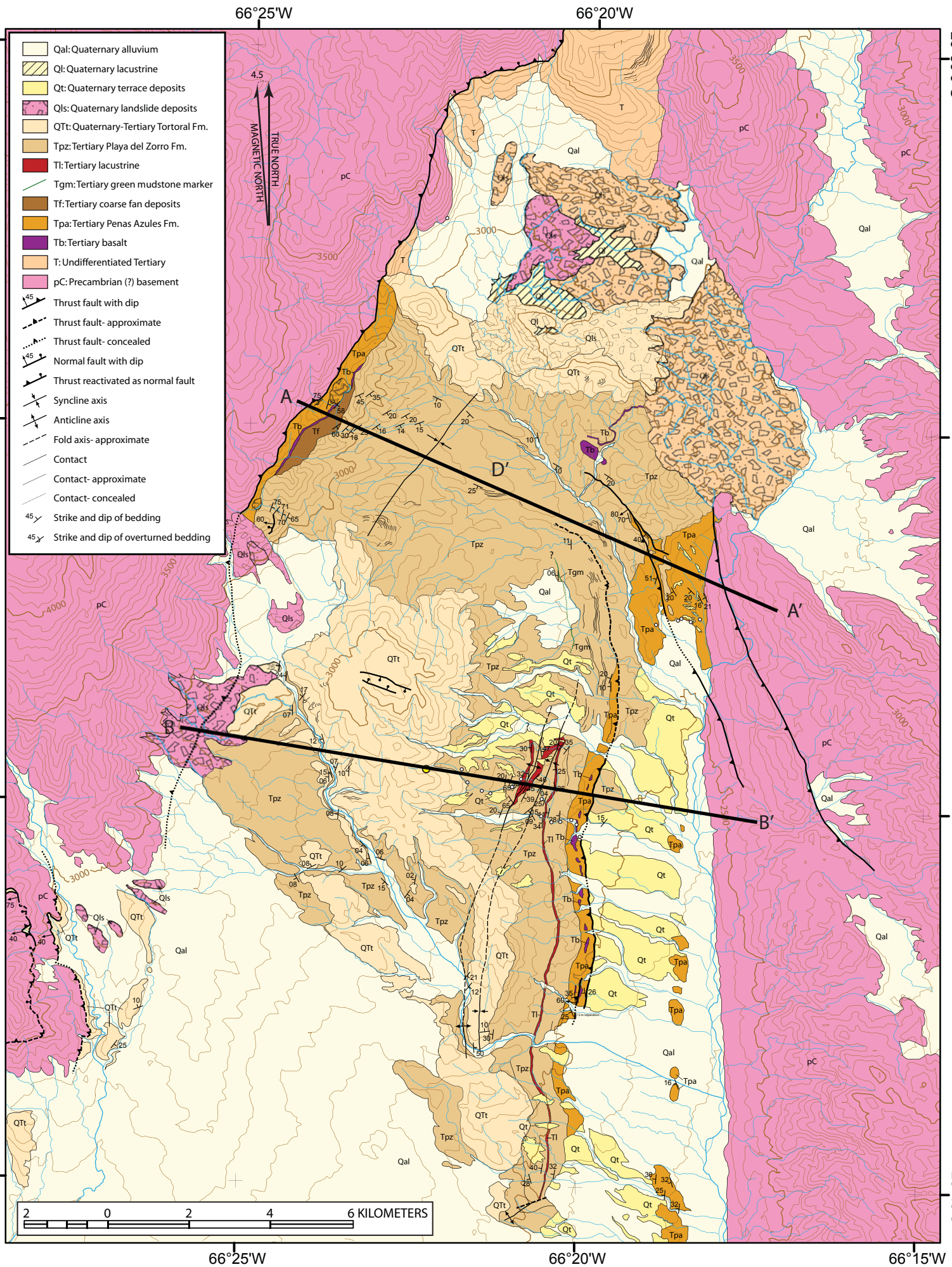

Fig. 5: Geological map of the El Cajon Basin as mapped by Lindsay Schoenbohm. Cross-section lines A-A' and B-B' are superimposed.

3.1 Northern Cross-section A-A' (Fig. 6a)

The cross-section line is 13.6 km long and extends from the Sierra de Chango Real across the El Cajón Basin into the basement exposure of the Sierra de Quilmes. The cross-section is not vertically exaggerated, and is projected to 500m below sea level, covering a vertical range of 4000m. The map is rich with attitudes along the margins of the basin, but is relatively poor in the center where the Playa del Zorro Fm. is exposed. The cross-section line is relatively parallel to dip direction through the central fault block. The angle between the cross-section line and the dip of the faults on the eastern side of the basin is oblique as is the angle between the cross-section line and the dip of the sedimentary units between these two faults. All faults within the section are reverse, east vergent, basement-rooted faults. Fault dips are poorly constrained across the section line, and as such a conservative angle of 60° has been used to approximate a normal fault that has been reactivated based on. *Anderson*'s [1951] theory of faulting in which a normal fault will form at 60° along a line perpendicular to the direction of least stress, given a vertical primary stress. The dip of the fault within the Peñas Azules Fm. is 80° north of the section line, but the fault bifurcates before reaching the line, making the dip measurement unreliable for extrapolation into the section.

The basin is dominated by a southward-plunging, asymmetric syncline. The west dip of the axial plane is consistent with loading to the west. Along the western margin of the basin the Peñas Azules Fm. is overturned, dipping 75° W, against the Chango Real fault. The western outcrop the Peñas Azules Fm. contains a basalt layer in the upper half of the exposure and a thick fan overlying it which extends to the unit boundary. The thickness of the Peñas Azules on the western side of the basin is obscured by abutment against the Chango Real fault and overturning of the beds. The minimum thickness of the Peñas Azules

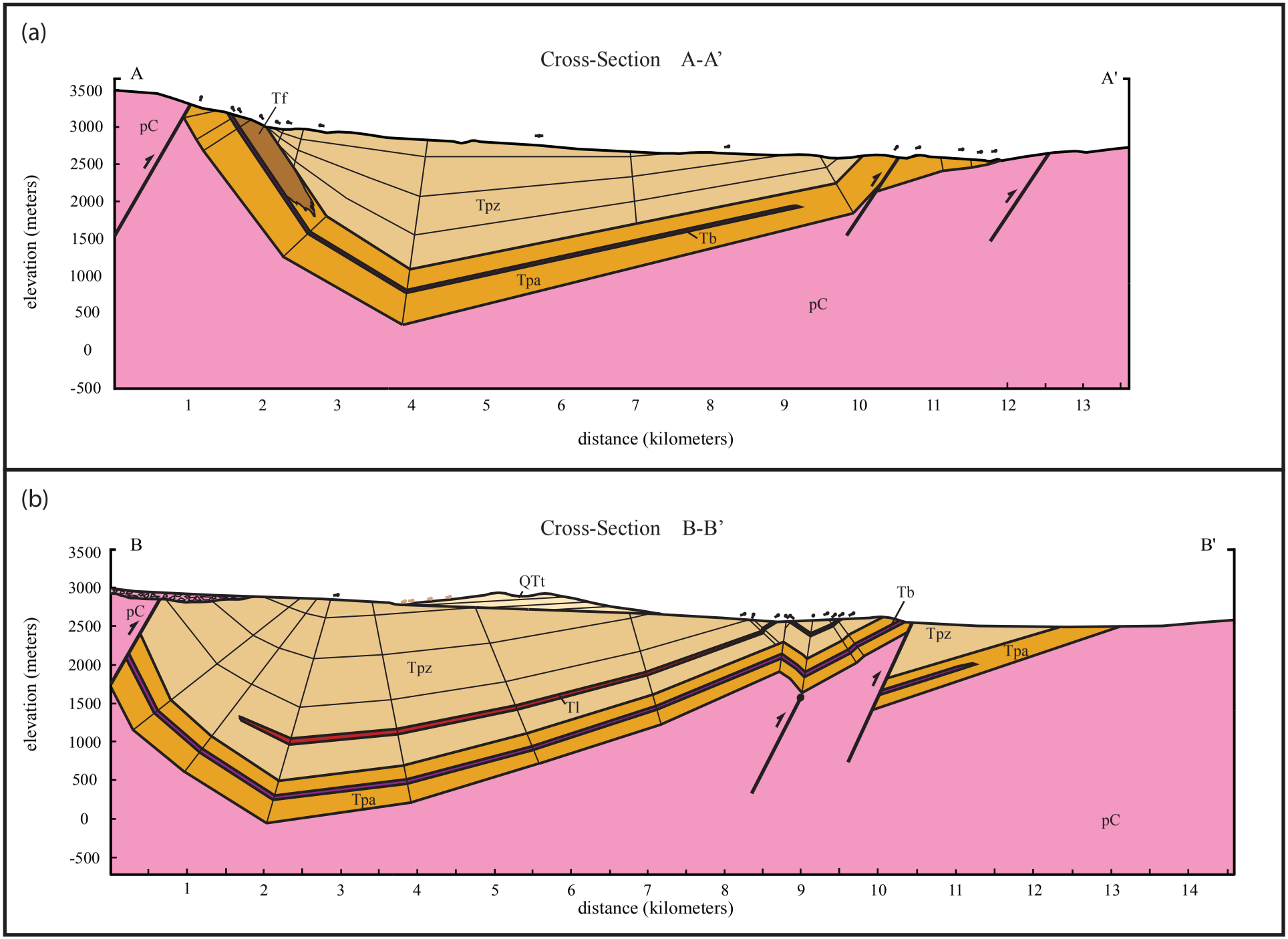

Fig 6. Cross-sections (a) A-A' & (b) B- B' depicting basin structure from the Sierra de Chango Real to the Sierra de Quilmes. A-A' is taken in the northern portion of the El Cajon & B-B' is taken in the middle portion of the El Cajon. See Fig. 4 for exact locations

on the western end of the basin is 900 m. The Peñas Azules Fm. crops up again in the eastern portion of the basin. The beds dip west at 51° as it approaches the middle fault. Immediately on the eastern side of the fault the dip shallows to 20° and dips SW, oblique with respect to the section line. Between the two eastern faults there is a small conformable cover of the Playa del Zorro Fm. that constrains the thickness of the Peñas Azules Fm. on the eastern side of the basin to ~300 m. The Peñas Azules Fm. therefore thins considerably from west to east across the basin, consistent with loading on the western end from the Sierra de Chango Real during the period of deposition. The basalt layer does not crop out on the eastern end suggesting it came from either the north or west and confirming loading to the west. The Playa del Zorro fm. exhibits growth structures on the western margin of the basin where it overlies the Peñas Azules fm. These features are absent on the easternmost outcrop of the Playa del Zorro on section A-A'. The strata thicken toward the synclinal hinge and thin to the east away from the hinge as is similar to trishear models of fault-propagation folds [Cardozo et al., 2003].

The high dip in the hanging wall of the middle fault, which is consistent along the fault to the north, does not match the low oblique dips on the footwall. This could be explained by the formation of a fault propagation fold, forming an anticline in a position now above the floor of the valley. The data however, do not support the formation of an anticline above the surface: the dip in the hanging wall would be expected to shallow towards the hinge and consequently towards the fault. Instead, the following is interpreted for the fault area. Basement uplift first occurred at the easternmost fault and the overlying strata deformed in response, shallowing towards the hinge of a forming anticline. Further into the hanging wall, the strata steepened in response to the localized uplift to the east. Stress

accumulated on the western margin of the uplift where the strata were incurring the greatest folding and resulted in the formation of the second fault to accommodate further uplift and shortening. In this model, uplift along the eastern margin of the basin began with the central uplift of the Sierra de Quilmes, which then propagated away from the central point into the El Cajón Basin.

3.2 Middle Cross-section B-B' (Fig. 6b)

The second cross-section is taken through the middle of the El Cajón Basin. The line is 14.6 km long and again extends from the Sierra de Chango Real to the Sierra de Quilmes. The section is not vertically exaggerated, and falls between the elevations of 3500 to – 550 km. The Peñas Azules fm. does not outcrop along the western margin of the basin. A Quarternary landslide deposit comprised of basement blocks and modern alluvium covers the contact between the basement and the sedimentary sequence on the western end. The formation outcrops in the eastern half of the basin against a fault and then again further east where it overlies the basement of the Sierra de Quilmes. The exact location of the easternmost Peñas Azules fm. is indeterminable due to Quaternary cover, but can be extrapolated following the pattern of outcrop from south of the line. Because of poor exposure in the western part of the cross section, a number of features of this cross section, including thickness of the Peñas Azules Fm. are inferred from the patterns observed in the seismic data to the south and in the cross section A-A'. The Playa del Zorro Fm exhibits growth strata along the western margin, but to a lesser extent than it does in the north of the basin. This interpretation is based on the larger amount of deformation seen at outcrop at A-A' than is seen near the Chango Real further to the south in the seismic data. Like in the

north, the formation thickens towards the syncline fold-hinge near the center of the basin. Extrapolation of strike and dip direction from the northern end of the basin and the southward plunge of the basin syncline lead to the interpretation that the Playa del Zorro fm. is in contact with the Chango Real fault at the surface and that the Peñas Azules is located at depth.

In the eastern part of the basin, the Playa del Zorro fm is folded into an anticline-syncline pair that exposes the lacustrine unit contained within the formation. The lacustrine unit dies out north of the section line, but extends along strike ~10 km to the south where it becomes obscured in Quaternary cover. This places the paleo-lake in the southern half of the basin, which could indicate that the northern portion of the basin was already higher in elevation when the lake existed. Neither the anticline nor the syncline exhibit a significant plunge, with attitudes near the hinges pointing both north and south depending upon the location. There is an isolated band of 65° dip just west of the fold. Field observations indicate that the high dip is extremely localized and occurs on a small scale, though it is traceable along strike. [Schoenbohm, pers. comm.] As such, this kink is not projected into the Peñas Azules Fm.

In the center of the basin the Tortoral fm. sits above an angular unconformity over the Playa del Zorro. The discordance in angle is slight at approximately 7° on the eastern end of the outcrop. This angle is presumably higher on the western end of the Tortoral fm. outcrop, but this is poorly constrained by surface data. The dip of the formation varies little throughout the basin, suggesting that it was deposited after the period of significant deformation.

The only exposed intra-basin fault across the section line is east of the anticline-syncline pair. Displacement along the fault is nearly 1 km for the base of the Peñas Azules Fm based on projection of surface dips to the fault at depth. A second fault is interpreted below the hinge of the syncline to explain the folding. The interpretation of the fault and folding in the subsurface is primarily based on the seismic data in the south. This is a fault propagation fold where the fault tip is still in the basement and the overlying sedimentary strata have not yet experienced brittle failure. The Playa del Zorro thickens in the hinge zones of the folds, but thins across the folds as a whole. The high angle basement-rooted reverse fault is interpreted to be uplifting basement rock with the sedimentary units more or less "draping" over the uplifted basement.

3.3 Campo del Arenal Seismic Data (Fig. 3) from *Mortimer et al, 2007*

The seismic lines of *Mortimer et al.* [2007] were taken at the southernmost extent of the El Cajón Basin and into the Campo del Arenal Basin near the southern edge of the exposed Sierra de Quilmes range. This study did not reevaluate the raw seismic data but relies on the interpretations made by *Mortimer et al.* [2007]. The sedimentary basin fill is divided into four sequences. Sequence 1 is correlated to the Peñas Azules Fm., Sequence 2 & 3 to the Playa del Zorro Fm. and Sequence 4 to the Totoral Fm. Each sequence boundary is defined by a significant reflector as described in detail in *Mortimer et al., 2007*.

The seismic sections show that Sequence 1, or the Peñas Azules Fm. is conformable with the basement, which is largely planar. All of the seismic sections show the sequences gently dipping to the west. The lines do not, however, cross or closely approach the Chango Real fault and so the basin fill architecture along the western margin cannot be seen. The

data along the eastern margin and into the Sierra de Quilmes shows the South Quilmes Structure, which is the subsurface continuation of the west-bounding west-dipping fault of the Sierra de Quilmes anticline south of the exposed range. Section lines ARG01593 and ARG01553 both show an east-dipping fault that *Mortimer et al.* [2007] do not call the South Quilmes Structure but clearly plays a role in the uplift of the Sierra de Quilmes at this latitude. These two faults define a small footwall block that resembles an inverted horst, which is being uplifted over on both the east and west sides. The seismic sections also indicate growth strata on the eastern side for the Playa del Zorro Fm and the Totoral Fm. This is shown for the Playa del Zorro Fm. in the cross-sections to the north, but not for the Totoral, due to limited presence along A-A' and B-B'. The formation of growth strata on the western side cannot be validated due to the limited western extent of the seismic lines.

The seismic sections are vertically exaggerated based on the rough estimate that a 1 second two-way travel time is approximately equal to a kilometer [Mortimer et al., 2007]. This makes the faults appear steeper than they are in reality. Nevertheless, the faults remain high angle and the sections show the prevalence of steep faulting in controlling basement uplift. Most importantly for the generation of cross-section B-B', the seismic sections show a consistent mode of folding in the hanging wall of the high angle reverse faults. The mode is that of the formation of an anticline along the fault on the hanging wall with the hinge removed a few kilometers from the fault. A developed syncline further into the hanging wall than the anticline is not present in most of the seismic sections but is present in ARG01587. This pattern was used to aid in the subsurface interpretation of the anticline-syncline pair in B-B'.

There remain a few discrepancies between the seismic sections and the surface-generated cross-sections A-A' and B-B', the largest of which is that the dips of each fault in the two fault pairs to the north are in the same direction. The seismic data show that most of the displacement occurs between fault pairs with opposite dip. However, since minor faults in the seismic often occur together with the same dip and basement fabric appears to be variable in the region, the interpretation to the north remains sensible. The other major discrepancy is in the fault pattern in A-A'. Nothing of that nature is seen in the seismic, where the strata dip at approximately the same magnitude and direction in the hanging wall as the fault. The interpretation provided fits the surface data, but does remain as somewhat of an anomaly.

4. U-Pb Geochronology.

10 tuff samples were strategically collected from throughout the stratigraphy of the El Cajón Basin for U-Pb age dating (Fig 4 & 7). The samples were crushed using a disk mill and separated using heavy liquids with Bromoform and Methylene Iodide. After the heavy liquid separation, the zircon fraction was run through a Frantz magnetic separator to remove the magnetic portion. The non-magnetic fractions were analyzed at the UCLA SIMS laboratory with the facility's CAMECA ims 1270 ion microprobe. Grains were handpicked from the samples, placing an emphasis on pink euhedral grains with adherent glass to preferentially select the youngest volcanic grains [Pers. comm., Axel Schmitt]. The grains were then mounted in epoxy and sectioned to expose grain interiors and were then polished with 1μm Al_20_3 and ultrasonically cleaned. An Au coat of approximately 10 nm was applied to all of the analyzed grains.

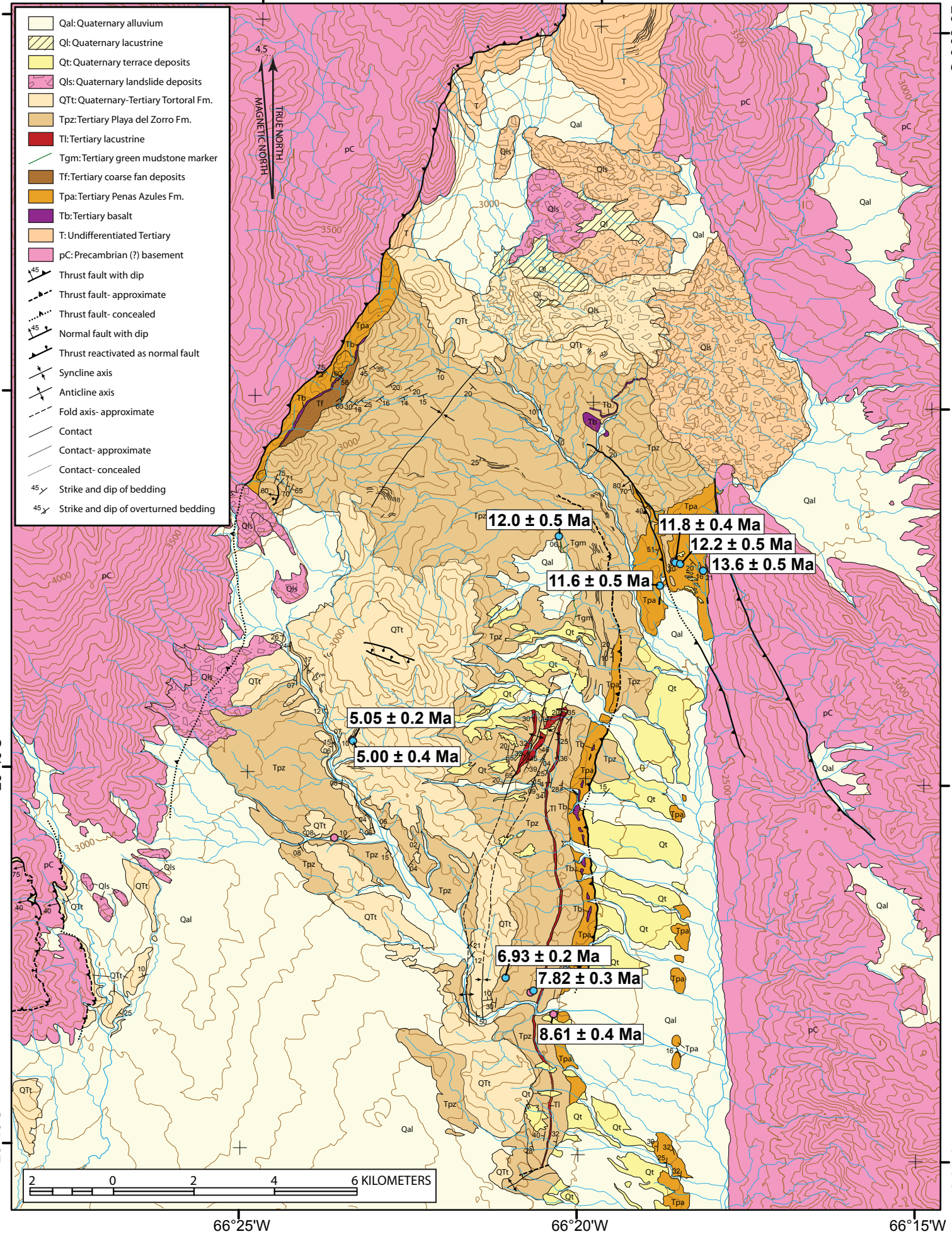

Fig. 7: Geological map of the El Cajon Basin as mapped by Lindsay Schoenbohm. U-Pb locations and ages are superimposed.

The zircon grain mounts were loaded into the ion microprobe and were probed using a 10-20 nA 16O- beam focused to a ~20-25μm diameter spot [Schmitt et al., 2003]. Since cathodeluminescence was not performed on the grains, the beam was focused on the tips of the grains to analyze the youngest portion of the grain. The ion microprobe was calibrated using AS-3 zircon standards with a technique similar to that of *Compston et al.* [1992]. Anywhere between 10-15 grains were run for each sample depending on the consistency of the preliminary ages returned during the sample analysis. $^{238}U/^{206}Pb$ ages were calculated using the U-Pb ratios by linear regression and computation of the weighted mean of each sample [Schmitt et al., 2003]. A $^{207}Pb/^{206}Pb$ correction was applied to correct for anthropogenic lead. The results are listed in Table 1.

One sample, E4, contains a large number of detrital zircons and has a weighted mean estimate of 8.61 ± .42 (2σ) Ma using only the two youngest grains. The remaining nine samples provided well-constrained ages and are applied to the stratigraphic column, with the exception of E9 , which by being near a fault has an uncertain position in the column and would not provide a meaningful increase in age resolution.(Fig. 3). From these results the base of the sedimentary sequence has been dated to 13.6 ± 0.5 Ma determined from the six youngest grains of tuff sample A5 above the basement contact. The maximum age of the Peñas Azules Fm. is approximately ~12.2 ± 0.5 Ma (A6) dated from a tuff bed below the Playa del Zorro Fm-Peñas Azules Fm. boundary and overlying the basalt layer based on an eight grain analysis. The basal age of the Playa del Zorro Fm is dated with a six grain analysis of a tuff bed lying slightly above the boundary of 12.0 ± 0.5 (T10) Ma. The boundary between the Playa del Zorro and Peñas Azules Formations is therefore tightly constrained between 12.0 and 12.2 Ma. E4 was taken from below the lacustrine bed and

sample	grain	spot	238U/206Pb	238U/206Pb	207Pb*/ 206Pb*	207Pb*/ 206Pb*	Correlation of T-W Concordia Ellipses	206/238 age [Ma]	±1σ [Ma]	U ppm	Th ppm	UO/U	% 206Pb*
A3	1	1	938.1	24.9	0.0529	0.0022	0.03	6.91	0.18	2368	421	7.9	99.1
A3	2	1	969.9	39.1	0.0594	0.0040	0.00	6.63	0.27	428	97	7.7	98.3
A3	3	1	968.1	30.5	0.0582	0.0029	-0.13	6.65	0.21	889	209	7.7	98.5
A3	4	1	897.7	33.1	0.0711	0.0046	0.01	7.05	0.27	426	112	7.8	96.8
A3	5	1	895.3	25.0	0.0506	0.0021	-0.07	7.26	0.20	1606	309	7.9	99.4
A3	6	1	924.2	26.9	0.0533	0.0017	-0.01	7.01	0.20	3648	955	7.8	99.1
A3	7	1	953.3	26.5	0.0520	0.0020	0.17	6.81	0.19	1783	413	7.9	99.3
A3	8	1	913.2	30.4	0.0510	0.0034	0.06	7.10	0.24	916	356	7.8	99.4
							w.m.	**6.93**					
							±1σ	**0.08**					
							MSWD	**0.98**					
							n	**8**					
A5	1	1	508.4	14.9	0.0511	0.0031	-0.04	12.68	0.38	398	132	7.8	99.4
A5	2	1	474.4	13.2	0.0491	0.0012	-0.01	13.62	0.38	1686	670	7.7	99.6
A5	3	1	444.6	14.9	0.0607	0.0053	0.00	14.30	0.50	289	135	7.6	98.2
A5	4	1	476.0	12.9	0.0486	0.0016	0.04	13.59	0.37	1057	247	7.8	99.7
A5	5	1	469.9	15.0	0.0526	0.0017	0.09	13.68	0.44	1058	603	7.7	99.2
A5	6	1	457.5	12.9	0.0668	0.0019	-0.13	13.80	0.40	1214	388	7.6	97.4
							w.m.	**13.5**					
							±1σ	**0.2**					
							MSWD	**1.63**					
							n	**6**					
A6	1	1	512.8	20.4	0.0501	0.0037	0.46	12.58	0.50	555	288	7.7	99.5
A6	2	1	545.9	18.7	0.0485	0.0026	0.12	11.85	0.40	606	287	7.7	99.7
A6	3	1	493.6	15.3	0.0638	0.0024	-0.05	12.85	0.41	593	220	7.6	97.8
A6	4	1	536.8	16.4	0.0520	0.0030	0.21	12.00	0.37	361	170	7.6	99.3
A6	5	1	539.4	16.6	0.0541	0.0030	-0.09	11.91	0.37	447	216	7.6	99.0
A6	6	1	505.3	19.7	0.0593	0.0040	0.18	12.62	0.50	294	128	7.7	98.3
A6	7	1	461.7	22.8	0.0472	0.0038	0.07	14.02	0.69	530	255	7.5	99.9
A6	8	1	555.9	17.8	0.0501	0.0020	-0.19	11.62	0.37	583	250	7.8	99.5
							w.m.	**12.2**					
							±1σ	**0.02**					
							MSWD	**2.11**					
							n	**8**					
T10	1	1	491.2	15.4	0.0862	0.0042	-0.23	12.51	0.42	1183	1009	7.4	94.9
T10	2	1	554.0	17.2	0.0588	0.0038	0.17	11.53	0.36	295	100	7.7	98.4
T10	3	1	538.5	20.9	0.0810	0.0074	-0.25	11.52	0.48	321	140	7.3	95.6
T10	4	1	530.5	12.8	0.0450	0.0026	0.11	12.25	0.29	638	246	7.8	100.2
T10	5	1	510.7	20.3	0.0551	0.0043	-0.25	12.56	0.51	285	87	7.6	98.9
T10	6	1	539.1	17.4	0.0643	0.0037	0.31	11.77	0.39	427	145	7.7	97.7
							w.m.	**12.0**					
							±1σ	**0.2**					
							MSWD	**1.29**					
							n	**6**					

Table 1: Data from zircon analyses. Data in red was not included for the calculation of the weighted mean (w.m.), standard deviation or the MSWD.

EC9	1	1	470.4	23.0	0.0572	0.0082	-0.09	13.6	0.7	373	256	8.1	98.6
EC9	2	1	370.5	38.3	0.0736	0.0183	-0.04	16.9	1.8	280	156	7.4	96.5
EC9	3	1	376.5	34.2	0.0707	0.0091	0.12	16.6	1.6	542	320	7.2	96.9
EC9	4	1	540.5	23.1	0.0546	0.0049	0.01	11.8	0.5	1220	1635	8.5	98.9
EC9	5	1	620.3	41.6	0.0937	0.0132	0.11	9.8	0.7	243	135	8.2	93.5
EC9	6	1	504.5	23.6	0.0613	0.0069	0.32	12.6	0.6	428	254	8.8	98.1
EC9	7	1	220.7	9.3	0.5095	0.0138	0.05	12.0	1.5	440	293	8.9	40.8
EC9	8	1	517.9	22.5	0.0765	0.0094	0.02	12.0	0.6	382	213	8.8	96.1
EC9	9	1	525.8	24.9	0.0798	0.0083	0.4	11.7	0.6	391	868	8.9	95.7
EC9	10	1	571.1	24.9	0.0741	0.0113	-0.09	10.9	0.5	345	337	8.6	96.4
EC9	11	1	297.1	10.5	0.3967	0.0151	0.04	12.0	0.9	707	1058	9.1	55.2
EC9	12	1	538.2	22.8	0.0790	0.0105	0.03	11.5	0.5	345	221	8.9	95.8
EC9	13	1	521.9	27.5	0.0767	0.0130	0.19	11.9	0.7	211	241	8.9	96.1
EC9	14	1	425.0	25.8	0.2041	0.0182	0.21	12.2	1.0	150	131	8.6	79.8
							w.m.	**11.64**					
							±1σ	**0.19**					
							MSWD	**1.23**					
							n	**11**					
E12	1	1	430.7	18.4	0.0754	0.0056	0.02	14.50	0.60	858	243	8.6	96.3
E12	2	1	758.2	53.3	0.3894	0.0280	-0.34	4.83	0.79	1517	1580	8.5	56.1
E12	3	1	1191.6	47.3	0.0443	0.0049	0.37	5.51	0.22	2197	743	8.9	100.2
E12	4	1	1345.0	66.9	0.0852	0.0124	-0.33	4.58	0.25	833	1536	8.9	95.0
E12	5	1	541.4	24.7	0.4772	0.0196	0.11	5.33	0.68	600	1615	9.0	44.9
E12	6	1	1150.9	75.1	0.1916	0.0190	0.00	4.61	0.40	344	404	9.1	81.4
E12	7	1	569.2	35.3	0.4767	0.0245	-0.11	5.10	0.91	349	796	8.8	44.9
E12	8	1	1265.5	96.6	0.1654	0.0469	-0.07	4.30	0.49	150	420	9.0	84.8
E12	9	1	515.7	26.1	0.4984	0.0233	-0.02	5.31	0.82	189	287	8.9	42.2
							w.m.	**5.00**					
							±1σ	**0.14**					
							MSWD	**1.69**					
							n	**8**					
E11	1	1	1318.2	57.5	0.0725	0.0057	-0.06	4.82	0.22	1029		8.8	96.9
E11	2	1	896.9	37.4	0.0787	0.0070	0.01	6.98	0.31	510		9.1	95.8
E11	3	1	12.5	0.5	0.0573	0.0009	-0.02	495.00	19	298		9.0	1000.0
E11	4	1	1160.5	44.6	0.0629	0.0032	0.03	5.52	0.21	2178		9.0	97.9
E11	5	1	13.5	0.5	0.0574	0.0011	0.10	549.00	15	317		9.5	99.8
E11	6	1	13.4	0.5	0.0587	0.0015	-0.08	462.00	18	161		9.5	99.7
E11	7	1	19.8	0.7	0.0553	0.0010	0.01	317.00	11	504		9.5	99.7
E11	8	1	13.0	0.5	0.0570	0.0006	-0.02	477.00	18	478		9.0	100.0
E11	9	1	104.0	5.4	0.7702	0.0054	-0.03	4.66	4.51	2924		8.7	7.4
E11	10	1	1223.8	43.7	0.0743	0.0034	0.05	5.18	0.19	2200		9.2	96.4
E11	11	1	1248.6	49.4	0.1332	0.0079	0.18	4.65	0.21	1560		9.0	88.9
E11	12	1	13.4	0.5	0.0570	0.0010	0.05	465.00	17	232		9.2	99.9
E11	13	1	1078.4	41.9	0.0665	0.0054	0.03	5.91	0.24	1036		9.0	97.4
E11	14	1	520.8	23.3	0.1167	0.0122	-0.12	11.33	0.59	166		9.0	91.0
E11	15	1	488.8	21.2	0.0731	0.0089	-0.32	12.79	0.60	161		9.0	96.6
							w.m.	**5.05**					
							±1σ	**0.1**					
							MSWD	**2.51**					
							n	**5**					

E4	1	1	8.9	0.4	0.0948	0.0016	0.05	658.46	32.98	478		8.5	95.7
E4	2	1	456.4	21.9	0.0666	0.0056	0.16	13.83	0.68	264		8.7	97.4
E4	3	1	511.8	22.3	0.0625	0.0037	-0.02	12.38	0.55	524		8.7	97.9
E4	4	1	718.9	30.5	0.0743	0.0040	0.07	8.72	0.38	876		8.8	96.4
E4	5	1	12.7	0.5	0.0575	0.0009	-0.01	488.55	20.26	347		8.7	99.9
E4	6	1	5.7	0.3	0.0733	0.0007	-0.02	1045.69	43.37	206		8.8	100.1
E4	7	1	486.6	22.7	0.3470	0.0139	0.05	8.23	0.70	157		8.9	61.5
E4	8	1	463.6	19.3	0.0487	0.0024	-0.01	13.94	0.58	786		8.8	99.7
E4	9	1	502.5	18.5	0.0949	0.0034	0.01	12.03	0.48	1045		9.1	93.8
E4	10	1	504.5	24.0	0.0932	0.0070	0.02	12.07	0.62	428		8.5	94.0
E4	11	1	523.8	22.7	0.0664	0.0051	0.09	12.05	0.54	571		8.7	97.4
E4	12	1	18.4	0.7	0.0528	0.0003	0.01	340.67	13.36	5029		8.8	100.1
E4	13	1	13.3	0.6	0.0573	0.0006	0.01	466.65	19.17	433		8.8	99.9
E4	14	1	421.4	19.7	0.0935	0.0066	0.17	14.45	0.73	312		8.6	94.0
E4	15	1	446.0	20.5	0.0873	0.0068	-0.09	13.76	0.68	161		8.9	94.8
E4	16	1	443.3	20.8	0.0630	0.0044	0.06	14.30	0.69	371		8.6	97.9
E4	17	1	502.3	22.0	0.0600	0.0035	-0.02	12.68	0.56	521		8.8	98.2
							w.m.	**8.61**					
							±1s	**0.34**					
							±2s	**0.42**					
							MSWD	**0.39**					
							n	**2**					

E7	1	1	573.1	28.6	0.0869	0.0092	0.02	10.72	0.58	617	572	8.2	94.8
E7	2	1	548.5	29.5	0.0800	0.0094	-0.14	11.31	0.65	370	247	8.4	95.7
E7	3	1	547.9	25.8	0.0632	0.0070	0.14	11.58	0.56	462	296	8.6	97.8
E7	4	1	523.0	21.3	0.0772	0.0079	-0.29	11.90	0.52	391	283	8.9	96.0
E7	5	1	530.2	22.5	0.0620	0.0077	-0.19	11.98	0.53	377	266	9.1	98.0
E7	6	1	520.3	25.0	0.0670	0.0073	-0.06	12.14	0.61	320	200	7.8	92.8
E7	7	1	503.3	20.6	0.0773	0.0066	0.03	12.36	0.54	459	360	8.9	96.0
E7	8	1	458.7	24.2	0.0940	0.0096	0.07	13.27	0.76	331	199	8.9	93.9
E7	9	1	470.4	23.0	0.0572	0.0082	-0.09	13.58	0.68	347	195	7.3	93.9
E7	10	1	383.6	18.0	0.1726	0.0153	-0.01	14.09	0.86	421	899	8.7	83.9
E7	11	1	370.5	38.3	0.0736	0.0183	-0.04	16.86	1.84	377	183	8.3	97.3
							w.m.	**11.75**					
							±1s	**0.21**					
							MSWD	**0.95**					
							n	**7**					

though the age of 8.61 ± .42 (2σ) Ma is only a maximum age of two grains, it is the best lower bracketing age obtained for the lacustrine bed. A tuff bed from above the lacustrine bed provides a minimum age for the upper end of the lacustrine bed of 7.82 ± 0.32 Ma (A1, 6 grains). These two ages tenuously bracket the lacustrine bed between 7.82 ± 0.32 Ma and 8.61 ± .42 (2σ) Ma. The top of the Playa del Zorro Fm has a maximum age of 6.93 ± 0.15 Ma from an ash (A3) below the contact with the Totoral Fm. using the youngest eight probed grains. The contact between the Playa del Zorro and the Totoral Formations is not well constrained due to a lack of ash from the base of the Totoral. The top of the Totoral Fm. exposure is dated to 5.00 ± 0.42 Ma (E12, 8 grains). As this age carries significance for understanding the interplay between climate and tectonics in the region, this study confirmed this age by dating a second tuff bed slightly below E12. Analysis of this bed (E11, 5 youngest grains) produced an age of 5.05 ± 0.21 (2 σ), confirming the previous age.

5.1 North-South Deformation Age Constraints

The Juan de Fernandez ridge with the South American subduction margin should cause a north to south sequence of deformation. Some portions of the El Cajón Basin are consistent with this prediction, whereas others are not. The first line of evidence comes from the Peñas Azules Fm. The Peñas Azules Fm. is thicker in the north of the basin than it is in the south. This is well evidenced in the Campo del Arenal Basin from the seismic data of *Mortimer et al.* [2007]. Four sections (ARG01555, ARG01587, ARG01553 & ARG01551) show from north to south decrease in thickness along the strike of the Chango Real reverse fault. Across a span of ~18 km the Peñas Azules Fm. decreases in thickness from ~700 to ~400 m based on a 1 sec TWTT to 1km approximation. To the north on section line A-A',

along the Chango Real fault, the Peñas Azules has a minimum thickness of 900 m while a true thickness is obscured by the overturning of the beds. With transport direction to the east in the Peñas Azules [Bossi et al., 2000] the factors effecting thickness along strike are limited to sediment supply and accommodation space, for which an increase of either within the regional context implies uplift and loading along the Chango Real. The increased thickness to the north is interpreted to be a result of accommodation space opening first in the north by loading along the Chango Real fault and then propagating to the south, allowing less deposition of the Peñas Azules Fm.

On the east side of the basin, the uplift of Sierra de Quilmes also propagated from north to south. Paleocurrent directions shifted from being dominantly E in the Peñas Azules Fm. to being SE in the Playa del Zorro [Bossi et al., 2000]. This shift indicates that in the northern portions of the El Cajón a transport barrier was emplaced on the eastern side of the basin. The barrier could not have extended as far south at the Quilmes does today, however, or drainage would have shifted to the south as it did later during deposition of the Totoral Fm, as indicated by the south-flowing paleocurrent directions [Bossi et al., 2000]. The location in which the basalt layer is found could indicate a steeper gradient in the north of the basin. Though sediment transport had not been cut off to the eastern portion of the basin at the time the basalt flowed into the basin, it did not flow east, following the direction of mean basin sediment transport, but instead diverted to the southeast, indicating there may have been increased topography in the northeastern sector of the basin at that time, possibly because of early uplift of the Sierra de Quilmes. Unfortunately exposure is limited in the northernmost part of the basin due to Quaternary cover. The presence of the lacustrine bed substantiates this further. It is contained within the Playa del Zorro Fm. and is completely

absent in A-A' suggesting that the Sierra de Quilmes had propagated to a position farther south than at the time of the deposition of the basalt flow. *Mortimer et al.* [2007] interpret that sediment transport was not blocked across the South Quilmes Structure until Sequence 3. Ambiguity between which sequence, 2, 3 or both, that *Bossi et al.* [2000] took their measurements from to determine paleocurrent direction does not allow adequate precision to deduce when the southern portion of the Sierra de Quilmes formed a barrier to transport relative to section line B-B'. However, it is reasonable to assume that the uplift followed the same pattern and propagated into the southern portion where the seismic sections lines lie after uplift began at B-B'. Using this reasoning, the uplift of the Sierra de Quilmes across A-A' can be estimated to be between 12.2 ± 0.5 Ma (the age of the basalt layer) and 8.61 ± 0.42 (2σ) Ma (the lower bracket of the lacustrine bed. Similarly for B-B', the bracketing of the lacustrine bed (7.82 ± 0.32 Ma to 8.61 ± 0.42 (2σ) Ma) is used to indicated the onset of uplift at this latitude.

5.2 East-West Deformation Age Constraints

Basin evolution from east to west is of greater significance to understanding plateau growth and how orogenic wedges evolve in a thick-skinned setting. Here the U-Pb geochronology provides insight into the timing of uplift for the Sierra de Chango Real and the Sierra de Quilmes across an E-W transect. In order to date the uplift of the Sierra de Chango Real, the age of the base of the Peñas Azules Fm. will be used. This is done assuming that deposition over the peneplain required loading along the Chango Real fault to generate the necessary accommodation space. The age generated from U-Pb zircon dating of 13.6 ± 0.5 Ma is a minimum age across the E-W trend where it is located due to its proximity

to the Chango Real fault, where deposition should be younger nearest to the loading and older further into the foreland.

To date the uplift of the Sierra de Quilmes the deposition of the lacustrine bed is used as an indicator of uplift as it interpreted to be formed from a switch to internal drainage, which would require an orographic barrier between the basin and the foreland drainage network. The lacustrine bed is bracketed between 7.82 ± 0.32 Ma and 8.61 ± .42 (2σ) Ma. The lower bracket is statistically weak but is a plausible age given its location in the stratigraphy and that the youngest grains in a sample provide a maximum age for that sample (Pers. comm., Axel Schmitt). The age bracket of 7.82-8.61 Ma provides a minimum age for the uplift of the Sierra de Quilmes along the E-W transect where the tuff samples were collected. Uplift ages may vary from younger to the north to older to the south. This is due to the fact that an effective orographic barrier is not likely to form until the more resistant basement is exhumed [Sobel et al., 2003], therefore there is a lag time between the uplift of the Sierra de Quilmes and the formation of the lacustrine bed.

Exhumation of the Sierra Aconquija has been dated by *Sobel & Strecker* [2003] to occur between 4.5 & 5.5 Ma based on apatite fission-track thermochronology. This age likely post-dates the onset of uplift at the Sierra Aconquija and *Sobel & Strecker* [2003] apply an age of ~6 Ma to this onset.

6. Basin Evolution

The El Cajón Basin began forming ~13.6 Ma when uplift and loading occurred at the Sierra de Chango Real along a high-angle reverse fault that was most likely a reactivated normal fault from the Cretaceous rifting event. The loading caused flexural subsidence in the

foreland in agreement with basin models [Decelles & Giles, 1996] allowing deposition of the Peñas Azules Fm over the basement peneplain with a mean transport direction to the east [Bossi et al., 2000]. While there is no evidence of significant deformation within the basin during the deposition of the Peñas Azules Fm., the distribution of the basalt flow indicates increased topography in the northeastern most part of the basin, which may be an expression of exhumation and uplift of the Sierra de Quilmes basement anticline in this area at ~12.2 Ma. By ~12 Ma the Playa del Zorro Fm was being deposited and the depocenter had shifted further south along the Chango Real [Mortimer et al., 2007] with a mean transport direction deflected to the southeast [Bossi et al., 2000]. At ~8 Ma the expression of the Sierra de Quilmes has formed a barrier to sediment transport in the northern half of the El Cajón Basin as indicated by the presence of the lacustrine bed. During the deposition of the younger portion of the Playa del Zorro (Sequence 3), the El Cajón Basin had been effectively compartmentalized from the foreland, though transport may have continued from the Campo del Arenal to the Santa María [Mortimer et al., 2007]. Deformation within the basin appears to mirror the timing of uplift of the Sierra de Quilmes by accommodating the flexurally driven uplift. In the El Cajón the fault pairs are at least as young as the Playa del Zorro Fm. as determined from crosscutting relationships. In the Campo del Arenal, faulting cuts through the Totoral Fm. but this is not seen in the north, though erosion could be responsible. Deposition ceased at ~ 7 Ma and a period of erosion ensued. At ~6 Ma the Sierra Aconquija began uplifting east of the El Cajón, compartmentalizing the Santa María Basin from the foreland. Deposition resumed with the syntectonic Totoral Fm. massive fan conglomerate over an angular unconformity with the Playa del Zorro Fm [Mortimer et al., 2007]. By this time the Sierra de Quilmes uplift had propagated far enough south to divert sediment

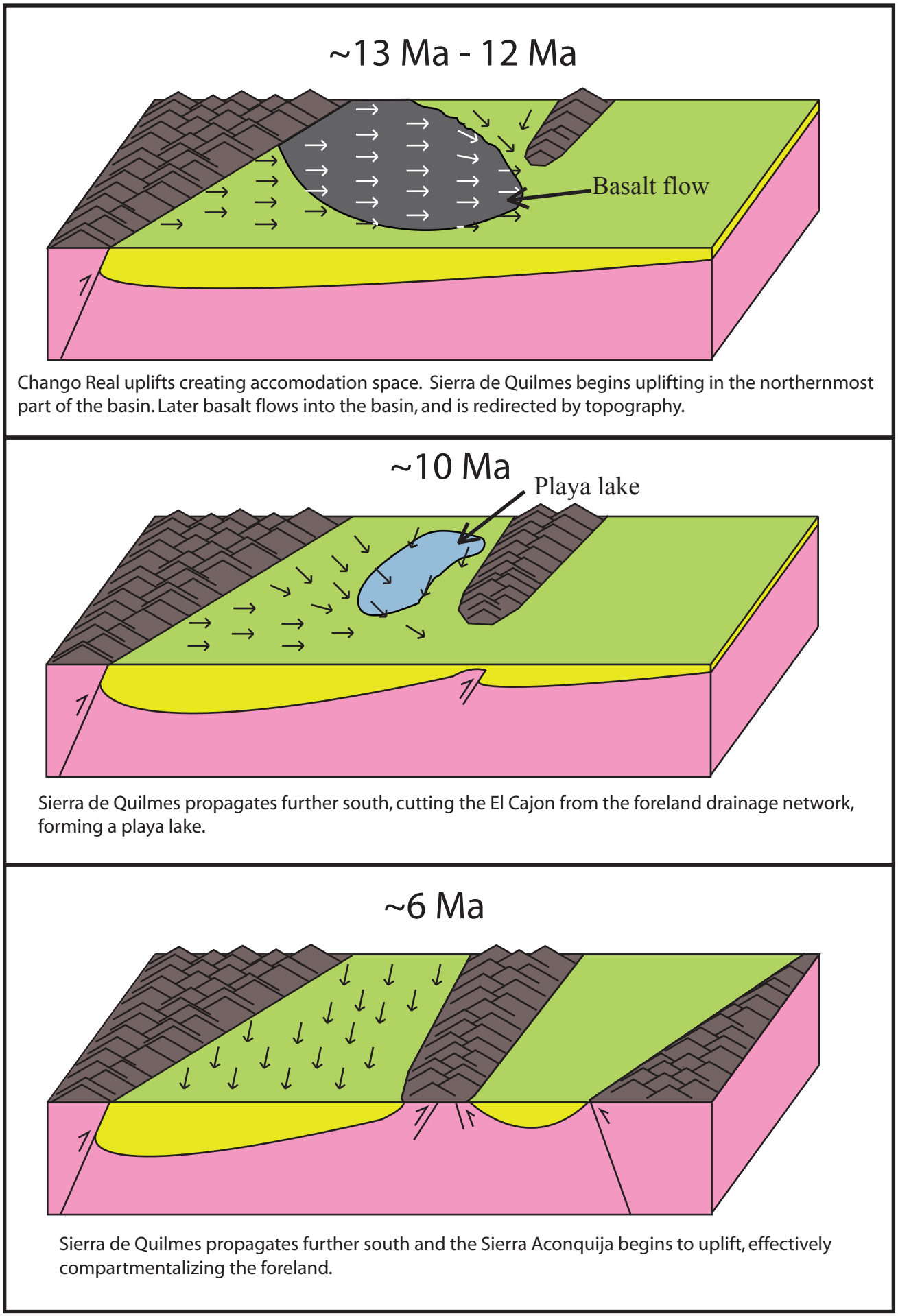

Fig. 8: Proposed model for basin evolution. Yellow represents undifferentiated basin fill, pink is basement rock and the brown represents topographic expression of the ranges. Superimposed on the basin are schematic paleocurrent directions that fit both the mean paleocurrent of *Bossi et al, 2000* for the unit deposited at the corresponding time and interpreted evolution from this study.

transport to the south within the El Cajón Basin. Sometime after 5 Ma, erosion resumed and exhumed the El Cajón Basin, differentiating it from the morphologic plateau. Fragmentation of the foreland was therefore in-sequence from west to east, with the deformation occurring first in the north and propagating south. This scenario for basin evolution is simplified and illustrated in Fig. 8.

7. Discussion

The interpretation of in-sequence deformation is a correction of *Mortimer et al.* [2007] based on a more comprehensive dating of the basin-fill stratigraphy. These new dates push the uplift of the Sierra de Quilmes back ~2 my. This in turn forces an in-sequence pattern of deformation as the mode by which the foreland was fragmented, whereas *Mortimer et al.* [2007] had interpreted the uplift of the Sierra de Quilmes to occur after that of the Sierra Aconquija, creating an out-of-sequence pattern. They used the differential loading between the Sierra de Chango Real and the Sierra Aconquija to explain out of sequence deformation. In the scenario presented in this study, the N-S trend of the Sierra de Quilmes may be a result of flexural deformation being less controlled by basement fabric than the fault-controlled deformation of the Sierra de Chango Real and Sierra Aconquija. Faulting within the basin would then be a response to the anticline uplift, accommodating the flexure utilizing pre-existing structure. This explains the discontinuity throughout the basin of the intra-basin faults. However, this is conjecture and cannot be confirmed with the present data from the basin.

The new in-sequence interpretation more closely resembles the classic model of orogenic wedge propagation [Decelles & Giles, 1996]. This is especially true if the Sierra de

Quilmes is a flexural response to loading from one direction. Nevertheless, in this thick-skinned setting the mechanics of wedge propagation are significantly different than those in a thin-skinned setting. We do not see stacking of thrust sheets generating the ranges or associated loads that accommodate the formation of the intervening basins. Instead we see a much more important role for basement-cored structures in generating topography and fragmenting the foreland. The basement ranges are more resistant to erosion and block sediment transport, allowing sediment to accumulate in the intervening basins, incorporating them into the morphologic plateau. Pre-existing structures are also dominant in controlling faulting in this setting as can be seen in the El Cajón and the bounding ranges of the Hualfín-Santa María basin system. The variance in basement foliation is likely responsible for changing the vergence of faulting in the region, again emphasizing its importance.

The primary contribution of this study refined chronology for the stratigraphy in the El Cajón Basin. As has been demonstrated here, correct ages are critical for determining basin history, with implications for how these basins were formed relative to basins in thin-skinned settings. The cross-sections serve primarily to extend the data set present in the south in the form of seismic sections into the north where seismic data are lacking. Particularly, the combination of these two elements, the stratigraphic dating and the cross-sections allow a more complete understanding of the evolution of the El Cajón Basin. However, data are still insufficient to resolve all outstanding questions. In order to accurately constrain the evolution of this region, a greater spatial resolution is needed for both the tuff bed U-Pb ages and a comprehensive mapping of basement foliations in the ranges. These improved data sets would vastly increase understanding by allowing more concrete evidence the generalities used to explain the temporal & spatial evolution of the

ranges from N-S and by confirming or discounting the role of basement foliations in controlling fault vergence.

8. Conclusions

The El Cajón Basin contains a stratigraphy spanning from 5.0-13.6 Ma. This stratigraphy records the deformation of both bounding ranges, the Sierra de Chango Real and the Sierra de Quilmes. The new stratigraphic ages in unison with patterns of deformation and sedimentation show that the El Cajón Basin began forming 13.6 Ma from loading along the Chango Real reverse and was compartmentalized ~8 Ma by the north to south propagation of uplift of the Sierra de Quilmes anticline. The later uplift of the Sierra de Aconquija to the east at ~6 Ma [Sobel & Strecker, 2003] defines an in-sequence propagation of the orogenic wedge across the foreland of the Puna. The mechanism of this propagation varies greatly from that of a thin-skinned regime and is reliant upon the pre-existing structures from prior deformational periods that facilitate the formation of high-angle basement faults and basement uplift. Together the data show an expansion of the Puna Plateau through high-angle in-sequence deformation across the foreland generating basins that in-filled with sediment after transport to the foreland drainage network had been blocked.

REFERENCES

Anderson, E.M., 1951, *The dynamics of faulting*, 2nd ed., Oliver & Boyd, Edinburgh.

Bossi, G.E., Mauruaga, C.M., Georgieff, S.M., Ahumada, A.L., Ibañez, L.M. & Vides, M.E., 1997, The Santa María-Hualfín Neogene basin of the Pampean Ranges: An example of mixed tectonic evolution. *Memorias del I Congreso Latinoamericano de Sedimentologic*, v. 1, p. 97-104.

Bossi, G.E., Vides, M.E., Ahumada, A.L., Georgieff, S.M., Muruaga, C.M & Ibañez, L.M., 2000, Análisis de las paleocorrientes y de la varianza de los components a tres niveles, Neógeno del Valle del Cajón, Catamarca, Argentina. *AAS Revista*, v. 7, p. 23-47.

Cardozo, N., Bhalla, K., Zehnder, A.T. and Allmendinger, R.W., 2003, Mechanical models of fault propagation folds and comparison to the trishear kinematic model. *Journal of Structural Geology*, v. 25, p. 1-18.

Compston, W., Williams, I.S., Kirschvink, J.L., Zichao, Z and Guogan, M.A. 1992, Zircon U-Pb ages for the Early Cambrian time-scale. *Journal of the Geological Society, London*, v. 149, p. 171-184.

Dahlen, F.A., Suppe, J., and David, D., 1984, Mechanics of fold and thrust belts and accretionary wedges: cohesive Coulomb theory. *Journal of Geophysical Research*, v. 89, p. 10,087-10,101.

Davis, D., Suppe, J., and Dahlen, F.A., 1983, Mechanics of fold and thrust belts and accretionary wedges. *Journal of Geophysical Research*, v.88, p. 1153-1172

DeCelles, P.G. and Giles, K.A., 1996, "Foreland basin systems." *Basin Research*, v. 8, p. 105-123.

Garcia, P.E. and Davis, G.H., 2004, Evidence and mechanisms for the folding of granite, Sierra de Hualfín basement-cored uplift, northwest Argentina. *AAPG Bulletin*, v. 88, no. 9, p. 1255-1276.

Isacks, B., 1988, Uplift of the central Andean plateau and bending of the Bolivian orocline. *Journal of Geophysical Research*, v. 93, p. 3211-3231.

Mortimer, E., Carrapa, B., Coutand, I., Schoenbohm, L., Sobel, E.R., Gomez, J.S., & Strecker, M.R., 2007, Fragmentation of a foreland basin in response to out-of-sequence basement uplifts and structural reactivation: El Cajón-Campo de Arenal basin, NW Argentina. *GSA Bulletin*, v. 119, no. 5/6**,** p. 637-653.

Ramos, V.A., Cristallini, E.O. and Perez, E.J., 2002, The Pampean flat-slab of the Central Andes. *Journal of South American Earth Science*, v. 15, p. 59-78.

Ramos, V.A., 1977, Basement tectonics from Landsat imagery in mining exploration. *Journal of the Royal Geological Mineralogical Society*, v. 56, p. 43-256.

Schmitt, A.K., Grove, M., Harrison, T.M., Lovera, O., Hulen, J., and Walters, M., 2003, The Geysers – Cobb Mountain Magma System, California (Part 1): U-Pb zircon ages of volcanic rocks, conditions of zircon crystallization and magma residence time. *Geochimica et Cosmochimica Acta*, v. 67, no. 18, p. 3423-3442.

Schmitt, J.G., and Steidtmann, J.R., 1990, Interior ramp-supported uplift: Implications for sediment provenance in foreland basins. *Geological Society of America Bulletin*, v. 102, p. 494-501.

Sobel, E.R., Hilley, G.E. & Strecker, M.R., 2003. Formation of internally drained contractional basins by aridity-limited bedrock incision. *Journal of Geophysical Research*, v. 108, no. B7, 2344 p. 1-23.

Sobel, E.R. & Strecker, M.R., 2003, Uplift, exhumation and precipitation: tectonic and climatic control of Late Cenozoic landscape evolution in the north Sierras Pampeanas, Argentina. *Basin Research,* v. 15, no. 4, p. 1-21.

Suppe, 1985. J. Suppe *Principles of Structural Geology*, Prentice-Hall, Englewood Cliffs, NJ (1985).

Strecker, M.R., Cerveny, P., Bloom, A.L. & Malizia, D., 1989. Late Cenozoic tectonism and landscape development in the foreland of the Andes: Northern Sierras Pampeanas (26 °-28 °S), Argentina. *Tectonics*, v. 8, no. 3**,** p. 517-534.

Toselli, A.J., Rossi, J., Aceñolaza, F., 1985, Milonita de bajo grado de la megafracture de Sierras Pampeanas en la quebrada de La Rioja, Sierra de Velasco, Argentina. *4 Congreso Geológico Chileno (Antofagasta) Actas,* v. 1 (2), p. 159-171

Urreiztieta, M. de, Gapais, D., Le Corre, C., Cobbold, P.R., Rossello, E., 1996, Cenozoic dextral transpression and basin development at the southern edge of the Puna Plateau, northwestern Argentina. *Tectonophysics*, v. 254, p. 17-39.

Von Gosen, W., 1998, Transpressive deformation in the southwestern part of the Sierra de San Luis (Sierras Pampeanas, Argentina). *Journal of South American Earth Sciences*, v. 11, p. 233-264.